Robotica (2010) volume 28, pp. 869–884. © Cambridge University Press 2009
doi:10.1017/S0263574709990713

A simple walking strategy for biped walking based on an intermittent sinusoidal oscillator

Chenglong Fu†,‡,*, Feng Tan† and Ken Chen†,‡

†*State Key Laboratory of Tribology, Tsinghua University, Beijing 100084, P. R. China*
‡*Department of Precision Instruments and Mechanology, Beijing 100084, P. R. China*

(Received in Final Form: November 10, 2009. First published online: December 10, 2009)

SUMMARY

This paper presents a control algorithm for biped walking by extension of previous work in the fields of central pattern generator (CPG) and passive walking. The algorithm takes advantage of the passive dynamics of walking, assisting only when necessary with an intermittent sinusoidal oscillator. The parameterized oscillator is used to drive the hip joint; the triggering and ceasing of the oscillator during a walking cycle can be modulated by the sensory feedback. The results from simulation indicate a stable, efficient gait, and robustness against model inaccuracy and environmental variation. We also examine the effects of oscillator parameters and link parameters on the gait, and design a controller to suppress the bifurcation phenomenon based on the error of prior step periods.

KEYWORDS: Biped walking; Intermittent oscillator; Sensory feedback; Bifurcation suppressing.

1. Introduction

Despite the successive development of humanoid robots by Honda's engineers, some fundamental control problems about biped locomotion have still neither been addressed nor solved in a satisfactory way.[1] One of these challenging problems is how to control biped machines like biological systems, which seem to have a simple, but efficient and robust locomotion strategy.

Biological investigations suggest that locomotion in vertebrates, including human beings, is mainly generated by a rhythm generator (central pattern generator (CPG)) within the spinal cord. The CPG is defined as a neural circuit that can produce self-sustained patterns of behavior, and the implementation of the artificial CPG is usually achieved under the form, either of artificial neural networks,[2] or of explicitly differential equations.[3,4]

Afferent information from the periphery has an important influence on the CPG. Although many attempts have been made to investigate the CPG-based approach for legged locomotion, there are only a few studies on the modulation of the CPG to proprioceptive information through sensory inputs. Taga *et al.*[5] demonstrated that stable bipedal locomotion was achieved with appropriate neural connections and biologically based sensory feedback pathways. Fukuoka and Kimura *et al.*[6] modulated the phase of a neural oscillator based on the body angle to control a quadruped robot walking on rough terrain. Aoi *et al.*[7] used a phase oscillator model with phase reset methods for a compass biped. Morimoto *et al.*[8] adjusted the phase of joint trajectories by a coupled oscillator model. In these studies, passive dynamics of the robot have not been utilized since all active joints are actuated in the whole walking cycle; as a result, the walking pattern is neither efficient nor natural, which means that the robot consumes more energy than human beings and the walking pattern does not look like human walking. Biological investigations indicate that human beings also exploit passive motion to minimize energy expenditure during walking.[9] Therefore, combining CPG-based method with passivity of the robot would be interesting not only for more robust locomotion but also for effective human-like walking.[10–12]

Similarly, since biped walking is a result of interaction between a neural system and a musculo–skeletal system, it has been suggested that the synchronization property of the biped controller with the robot dynamics plays an important role in stable locomotion. Several studies synthesized joint trajectories as a function of a physical variable of the robot. Ono *et al.*[13] applied a negative feedback from the shank joint angle to the input torque at the thigh joint. Westervelt *et al.*[14] designed the walking controller by slaving the actuated joints to the underactuated variable. Geng *et al.*[15] presented a sensor-driven neural controller for a biped robot to realize fast dynamic walking. Fu *et al.*[16] proposed that the feedback controller of humanoid walking should be phase-dependent. However, these methods rely on substantial sensory feedback such as from uninterrupted sensing of link angles or foot pressures, and there are usually many parameters to be determined in the synchronization controllers.

In this study, we undertake the development of a simple, but efficient and robust walking strategy by combining CPG-based method with passive dynamics for a kneed biped robot with semicircular feet. We suggest that the output of oscillator is only used to actuate the hip joint to swing the leg; (1) we use a simple periodic function (sinusoid) as the output of oscillator; (2) we utilize the passive property of biped walking by ceasing the rhythmic signal intermittently after the swing leg is fully extended; as a result the walking is efficient; (3) we demonstrate that the synchronization of biped walking can be ensured only by triggering/ceasing the output of oscillator upon the event emitted by two touch sensors placed on the foot and the kneecap respectively; (4) since the oscillator is a sinusoid and only used to control the hip joint, the numbers of parameters are smaller than that used in the existing neural

* Corresponding author. E-mail: fcl@tsinghua.edu.cn

https://doi.org/10.1017/S0263574709990713 Published online by Cambridge University Press

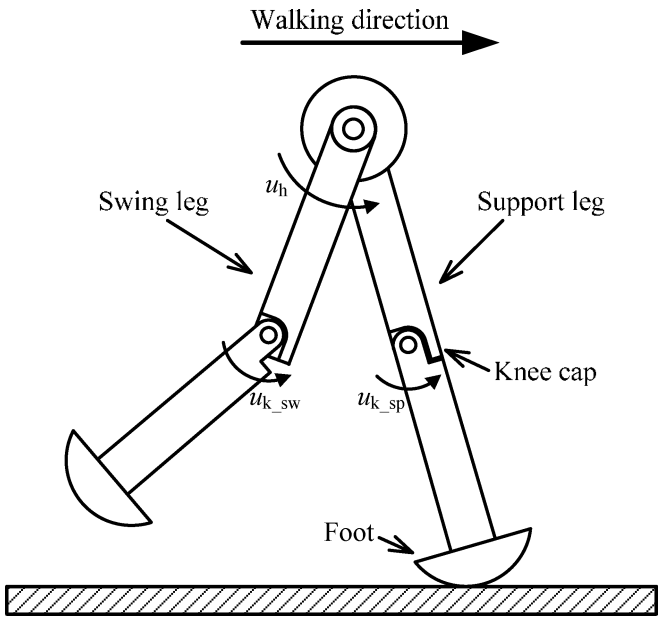


Fig. 1. The biped robot.

oscillator approach; and (5) results from simulation show that the proposed walking strategy has a good robustness against uncertainty both in oscillator parameters and physical parameters.

The rest of this paper is organized as follows. Section 2 describes a kneed biped model and introduces the analytical model. Section 3 describes the proposed walking strategy. Section 4 shows the typical features of steady locomotion. Section 5 conducts robustness against oscillator parameters, link parameters, and environment variation. Section 6 discusses the effect of parameters on various walking indices, and also designs a feedback controller to eliminate the bifurcation phenomenon. Finally, in Section 7, we conclude the paper.

2. Model of Kneed Biped Robot with Feet

2.1. Biped mechanism and basic hypotheses

As shown in Fig. 1, the four-link biped robot considered in this paper consists of two legs, which are connected at the hip joint. Each leg is composed of a thigh and a shank connected at a knee joint, which has a kneecap mechanism to prevent the leg from inverting. Both legs have arc-shaped feet that are rigidly attached to the shank, and the center of the arc is located on the shank. The ankle is not actuated then the robot is underactuated in single support phase. Two touch sensors are placed on the foot and the kneecap respectively in each leg. These sensors are used to synchronize the biped controller with the robot dynamics. The purpose of this study is to develop a simple, but efficient and robust locomotion strategy by active control through the hip and knee actuators.

The hypotheses assumed for the desired walking gait is now enumerated:

(H1) Walking consists of a single support phase and an instantaneous double support phase.[14]
(H2) The support leg is always straight during walking.
(H3) The swing leg is fully extended before the moment of ground contact.
(H4) The contact of the swing shank with the kneecap is assumed to be a completely inelastic collision.
(H5) The contact of the swing leg with the ground is also assumed to be a completely inelastic collision.[14]

Under above hypotheses, the single support phase can be divided into two phases from an aspect of the difference of the basic equation. As shown in Fig. 2, *the first phase* is from the start of the swing leg motion to collision at the knee; *the second phase* is from the knee collision to the touch down of the straight swing leg. The similar model and hypotheses were used by Ono *et al.*[13] and Harata *et al.*[17]

Figure 3(a) and (b) shows link parameters of the biped robot, where l_i denotes link length, a_i denotes the position of center of mass, r denotes foot radius, m_i denotes link mass, and I_i denotes inertia around mass center. Link parameters of the robot are shown in Table I.

2.2. Motion equations for phase 1 and phase 2

Under hypothesis (H2), the analytical model during the first phase can be represented as a three degrees-of-freedom (DOF) link system. As shown in Fig. 3(b), the generalized coordinates for phase 1 are defined as $(q_1, q_2, q_3)'$. The

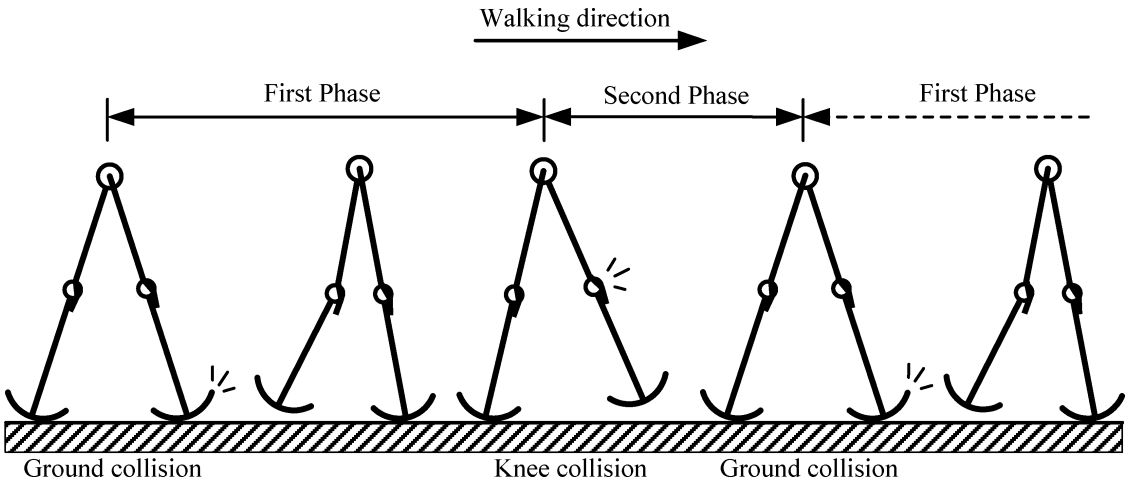


Fig. 2. Phases of biped locomotion.

https://doi.org/10.1017/S0263574709990713 Published online by Cambridge University Press

Table I. Physical parameter values for the robot.

Model parameters	Unit	Link	Label	Value
Mass	kg	Leg	m_1	3.30
		Thigh	m_2	2.20
		Shank	m_3	1.10
Length	m	Leg	l_1	0.70
		Thigh	l_2	0.35
		Shank	l_3	0.35
		Foot radius	r	0.20
Inertia at mass center	m^2 kg	Leg	I_1	0.154
		Thigh	I_2	0.032
		Shank	I_3	0.016
Center of mass	m	Leg	a_1	0.43
		Thigh	a_2	0.14
		Shank	a_3	0.18

equation of motion for phase 1 can be written as

$$\begin{bmatrix} D1_{11} & D1_{12} & D1_{13} \\ & D1_{22} & D1_{23} \\ sym & & D1_{33} \end{bmatrix} \begin{bmatrix} \ddot{q}_1 \\ \ddot{q}_2 \\ \ddot{q}_3 \end{bmatrix} + \begin{bmatrix} C1_{11} & C1_{12} & C1_{13} \\ C1_{21} & 0 & C1_{23} \\ C1_{31} & C1_{32} & 0 \end{bmatrix} \times \begin{bmatrix} \dot{q}_1 \\ \dot{q}_2 \\ \dot{q}_3 \end{bmatrix} + \begin{bmatrix} G1_1 \\ G1_2 \\ G1_3 \end{bmatrix} = \begin{bmatrix} u_{\mathrm{h}} \\ -u_{\mathrm{h}} + u_{\mathrm{k_sw}} \\ -u_{\mathrm{k_sw}} \end{bmatrix}, \tag{1}$$

where the elements $D1_{ij}$, $C1_{ij}$, and $G1_i$ of the matrices are shown in Appendix A. u_{h} and $u_{\mathrm{k_sw}}$ are torques applied at the hip and knee actuators as shown in Fig. 1. Similar equation has been used by Ono *et al*. [13], but signs of some elements of the equation in [13] are incorrect. The elements presented here are automatically derived by Symbolic Math Toolboxes in MATLAB.

Under hypothesis (H3), the analytical model during the second phase can be represented as a 2-DOF link system. As shown in Fig. 3(c), the generalized coordinates for phase 2 are defined as $(q_1, q_2)'$. Thus the motion equation for phase 2 becomes

$$\begin{bmatrix} D2_{11} & D2_{12} \\ sym & D2_{22} \end{bmatrix} \begin{bmatrix} \ddot{q}_1 \\ \ddot{q}_2 \end{bmatrix} + \begin{bmatrix} C2_{11} & C2_{12} \\ C2_{21} & 0 \end{bmatrix} \begin{bmatrix} \dot{q}_1 \\ \dot{q}_2 \end{bmatrix} + \begin{bmatrix} G2_1 \\ G2_2 \end{bmatrix} = \begin{bmatrix} u_{\mathrm{h}} \\ -u_{\mathrm{h}} \end{bmatrix}, \tag{2}$$

where the elements $D2_{ij}$, $C2_{ij}$, and $G2_i$ of the matrices are shown in Appendix B.

2.3. Equations governing knee collision and ground collision

Let $\boldsymbol{q}^-$, $\boldsymbol{q}^+$, $\dot{\boldsymbol{q}}^-$, and $\dot{\boldsymbol{q}}^+$ denote the pre- and post-impact generalized positions and generalized velocities, respectively. The superscript "−" and "+" will denote quantities immediately before and after impact thereinafter.

After the end of the first phase knee collision occurs when the shank comes in line with the thigh. Under hypothesis (H4), according to the angular momentum theorem, we can obtain

$$\boldsymbol{D}1(\boldsymbol{q}^+)\dot{\boldsymbol{q}}^+ - \boldsymbol{D}1(\boldsymbol{q}^-)\dot{\boldsymbol{q}}^- = \begin{bmatrix} 0 \\ -\hat{F}_{\mathrm{k}} \\ \hat{F}_{\mathrm{k}} \end{bmatrix}, \tag{3}$$

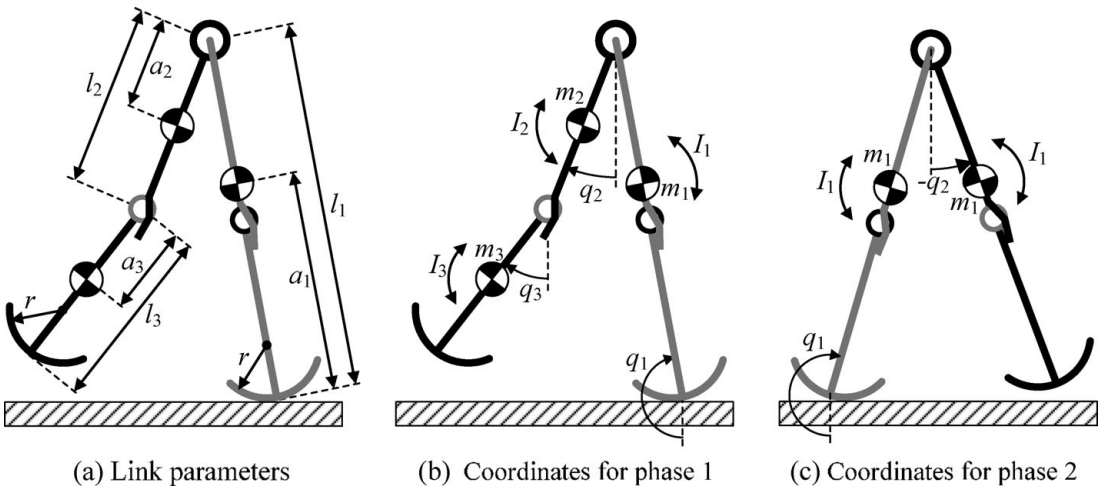
where $\hat{F}_{\mathrm{k}}$ is the integral of the torque acting on the shank during knee collision. After the collision, the angular velocities of the shank and thigh become same and therefore

$$[0 \ \ -1 \ \ 1]\dot{\boldsymbol{q}}^+ = 0. \tag{4}$$

Solving Eqs. (3) and (4) yields

$$\begin{bmatrix} \dot{\boldsymbol{q}}^+ \\ \hat{F}_{\mathrm{k}} \end{bmatrix} = \begin{bmatrix} \boldsymbol{D}1(\boldsymbol{q}^+) & \begin{bmatrix} 0 \\ 1 \\ -1 \end{bmatrix} \\ \begin{bmatrix} 0 & -1 & 1 \end{bmatrix} & 0 \end{bmatrix}^{-1} \begin{bmatrix} \boldsymbol{D}1(\boldsymbol{q}^-)\dot{\boldsymbol{q}}^- \\ 0 \end{bmatrix}. \tag{5}$$

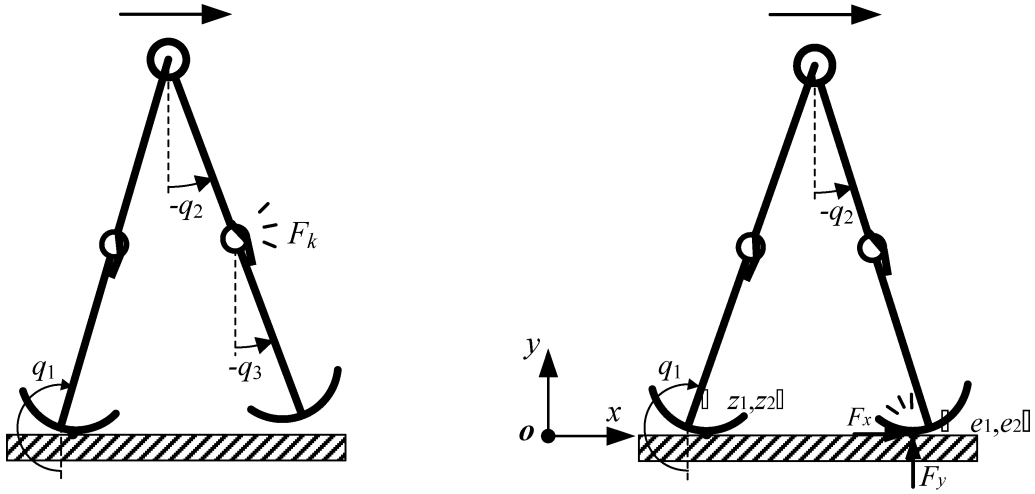
After the end of the second phase ground collision occurs when the swing foot touches the ground. The contact model



(a) Link parameters (b) Coordinates for phase 1 (c) Coordinates for phase 2

Fig. 3. Link parameters and coordinate definition of the biped robot.

https://doi.org/10.1017/S0263574709990713 Published online by Cambridge University Press



(a) Knee collision (b) Ground collision

Fig. 4. Impact model.

of ground collision requires the four DOF of the robot.[13] Select the generalized coordinates to be $\boldsymbol{q}_{\mathrm{f}} = [q_1, q_2, z_1, z_2]'$ as shown in Fig. 4. This gives once again a model of the form

$$\boldsymbol{D}_{\mathrm{f}}(\boldsymbol{q}_{\mathrm{f}})\ddot{\boldsymbol{q}}_{\mathrm{f}} + \boldsymbol{C}_{\mathrm{f}}(\boldsymbol{q}_{\mathrm{f}}, \dot{\boldsymbol{q}}_{\mathrm{f}})\dot{\boldsymbol{q}}_{\mathrm{f}} + \boldsymbol{G}_{\mathrm{f}}(\boldsymbol{q}_{\mathrm{f}}) = \boldsymbol{B}_{\mathrm{f}}(\boldsymbol{q}_{\mathrm{f}})\boldsymbol{u} + \left(\frac{\partial \boldsymbol{E}(\boldsymbol{q}_{\mathrm{f}})}{\partial \boldsymbol{q}_{\mathrm{f}}}\right)' \begin{bmatrix} F_x \\ F_y \end{bmatrix}, \tag{6}$$

where F_x and F_y are, respectively, the tangential and normal forces acting on the swing leg end at touchdown, $\boldsymbol{E}(\boldsymbol{q}_{\mathrm{f}}) = [e_1(\boldsymbol{q}_{\mathrm{f}}), e_2(\boldsymbol{q}_{\mathrm{f}})]'$ is the Cartesian coordinates of the point of the forward leg in contact with the ground surface (see Fig. 4b).

According to the angular momentum theorem, we can obtain

$$\boldsymbol{D}_{\mathrm{f}}(\boldsymbol{q}_{\mathrm{f}}^{+}) \cdot \dot{\boldsymbol{q}}_{\mathrm{f}}^{+} - \boldsymbol{D}_{\mathrm{f}}(\boldsymbol{q}_{\mathrm{f}}^{-}) \cdot \dot{\boldsymbol{q}}_{\mathrm{f}}^{-} = \left(\frac{\partial \boldsymbol{E}(\boldsymbol{q}_{\mathrm{f}})}{\partial \boldsymbol{q}_{\mathrm{f}}}\right)' \begin{bmatrix} \hat{F}_x \\ \hat{F}_y \end{bmatrix}, \tag{7}$$

where $\hat{F}_x = \int_{t^-}^{t^+} F_x(\tau)\,\mathrm{d}\tau$ and $\hat{F}_y = \int_{t^-}^{t^+} F_y(\tau)\,\mathrm{d}\tau$ are the results of integrating the contact impulse over the impact duration. Since the contact of the swing leg with the ground results in no rebound, we can obtain

$$\left.\frac{\partial \boldsymbol{E}(\boldsymbol{q}_{\mathrm{f}})}{\partial \boldsymbol{q}_{\mathrm{f}}}\right|_{\boldsymbol{q}_{\mathrm{f}}=\boldsymbol{q}_{\mathrm{f}}^{-}} \cdot \dot{\boldsymbol{q}}_{\mathrm{f}}^{+} = 0. \tag{8}$$

Solving Eqs. (7) and (8) yields

$$\begin{bmatrix} \dot{\boldsymbol{q}}_{\mathrm{f}}^{+} \\ \begin{bmatrix} \hat{F}_x \\ \hat{F}_y \end{bmatrix} \end{bmatrix} = \begin{bmatrix} \boldsymbol{D}_{\mathrm{f}}(\boldsymbol{q}_{\mathrm{f}}^{-}) & -\left(\dfrac{\partial \boldsymbol{E}(\boldsymbol{q}_{\mathrm{f}})}{\partial \boldsymbol{q}_{\mathrm{f}}}\right)'\Bigg|_{\boldsymbol{q}_{\mathrm{f}}=\boldsymbol{q}_{\mathrm{f}}^{-}} \\ \left.\dfrac{\partial \boldsymbol{E}(\boldsymbol{q}_{\mathrm{f}})}{\partial \boldsymbol{q}_{\mathrm{f}}}\right|_{\boldsymbol{q}_{\mathrm{f}}=\boldsymbol{q}_{\mathrm{f}}^{-}} & \begin{bmatrix} 0 & 0 \\ 0 & 0 \end{bmatrix} \end{bmatrix}^{-1} \times \begin{bmatrix} \boldsymbol{D}_{\mathrm{f}}(\boldsymbol{q}_{\mathrm{f}}^{-}) \cdot \dot{\boldsymbol{q}}_{\mathrm{f}}^{-} \\ \begin{bmatrix} 0 \\ 0 \end{bmatrix} \end{bmatrix}. \tag{9}$$

3. Walking Strategy

In previous studies, some researchers controlled all joints of biped robots. In this manner, for biped robots with multi-DOFs, the dimension is high, and many parameters have to be determined carefully; furthermore, the passive property of biped walking cannot be utilized. To solve this problem, we suggest that the walking strategy should take advantage of the passive dynamics of walking, assisting only when necessary with an intermittent oscillator. For the above biped model, we propose that an intermittent sinusoidal oscillator is used to drive the hip joint while the knee joints are driven by a simple control strategy. The triggering and ceasing of the intermittent oscillator are modulated by the sensory feedback during a walking cycle.

3.1. An intermittent sinusoidal oscillator for hip joint

Before we design the rhythmic signal for hip joint, we introduce an oscillator $Ae^{j\phi}$, where A is the amplitude that is constant and ϕ is the phase whose angular velocity, $\omega > 0$, is the angular frequency, that is,

$$\dot{A} = 0,\ \dot{\phi} = \omega. \tag{10}$$

Then, we design the hip torque u_{h} that is driven by the rhythmic signal. One of the simplest ways to design the rhythm signal is based on a sinusoidal function, which has the fewest parameters to represent periodic patterns. Therefore, we design the rhythmic signal as the simple function of amplitude A and phase ϕ of the oscillator and bias parameter B by

$$u_{\mathrm{h}}(t) = \begin{cases} A \cdot \sin\phi + B, & T_{\mathrm{G}}^{i} < t \le T_{\mathrm{K}}^{i}, \\ 0, & T_{\mathrm{K}}^{i} < t \le T_{\mathrm{G}}^{i+1}, \end{cases} \tag{11}$$

where $\phi = \omega \cdot (t - T_{\mathrm{G}}^{i}) + \phi_0$, T_{G}^{i} and T_{K}^{i} are time instants of ground collision and knee collision in the ith step respectively, and ϕ_0 is the initial phase of the oscillator.

The rhythmic signal is modulated by sensory inputs as follows. When the swing leg touches the ground, the oscillator receives a feedback signal from the touch sensor placed at the foot.[7] Instantly, the output is modified to restart

https://doi.org/10.1017/S0263574709990713 Published online by Cambridge University Press

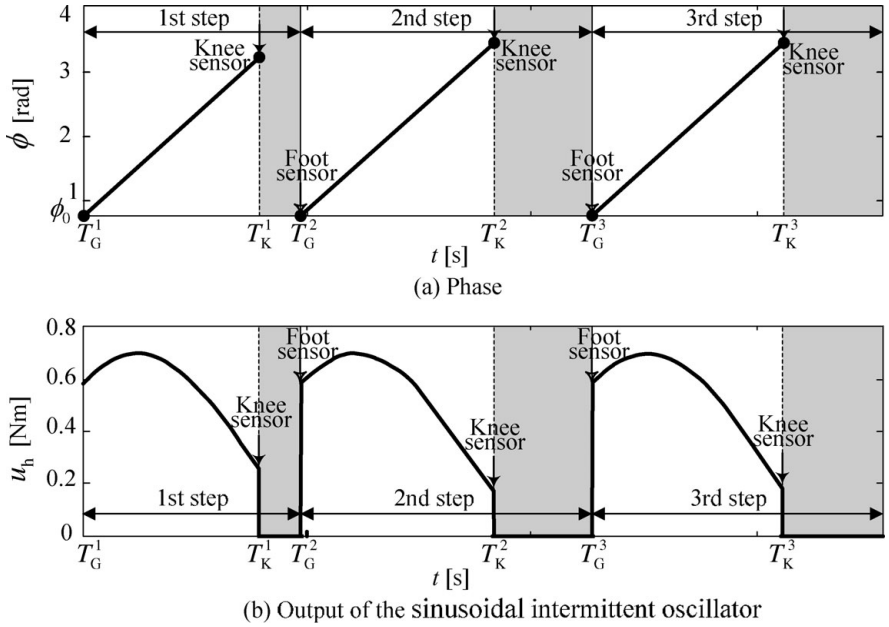


Fig. 5. Modulation of the intermittent oscillator due to feedback signals from foot sensor and knee sensor.

with a fixed value, and the initial phase of the oscillator is reset to a certain value ϕ_0 as shown in Fig. 5(a). When the swing leg is fully extended, the oscillator receives a feedback signal from the touch sensor placed at the kneecap. Instantly, the output ceases until the swing leg touches the ground, as shown in the shaded areas of Fig. 5. This intermittent control was inspired by the studies on the measurement of human electromyographic (EMG)[9] and the idea of quasi passive dynamic walking (PDW) conducted by Collins *et al.*[10,12] Timing of EMG in leg muscles during human walking indicates that the duration of activity of the most important leg muscles is intermittent.[9] Collins *et al.* validated this point of view by a physical biped robot which only generated an intermittent actuation in trailing ankle joint when the leading foot touched the ground. The walking pattern of this robot is efficient and natural.[10,12]

By triggering/ceasing the rhythmic signal upon the event emitted by above touch sensors, the synchronization of the controller with the robot dynamics can be achieved. The idea that the oscillator is switched off upon receiving the knee-lock signal is inspired by the work of Hobbelen and Wisse.[18] They pointed out that swing-leg retraction could improve disturbance rejection for limit cycle walkers. We assume that ceasing the input torque of the swing-hip joint before heel contact has the same effect as the swing-leg retraction. After the swing leg becomes straight, the robot is ready for landing with an appropriate posture. We expect that switching off the oscillator by the knee-lock signal could not only conserve efficiency but also improve robustness against environmental variation.

For the above design, there are only four parameters: amplitude A, angular frequency ω, bias B and reset phase ϕ_0; the numbers of parameters are smaller than that used in the existing neural oscillator approach.

3.2. *Control for knee joints*

As one of gait characteristics of human beings, walking with straight support legs is more efficient than with bent legs since energy requirements in muscles and motors are monotonically related to the torque at the joint. Since our biped robot is designed with a kneecap mechanism, a very simple control technique to keep the leg straight is to apply a constant torque C to the support knee joint by

$$u_{\text{k_sp}}(t) = C. \tag{12}$$

When the touch sensor placed at the foot detects the leg is in the support phase, the above control is triggered. This simple control technique can also be regarded as a monosynaptic stretch reflex in biological systems: when the muscle at the knee joint is stretched because of impact, sensory feedback causes an activation of the motoneurons innervating that muscle to counteract the imposed movement and support the weight of the body.[19]

The control action for the swing knee joint is designed as

$$u_{\text{k_sw}}(t) = \begin{cases} 0, & T_{\text{Ground}} < t \leq T_{\text{Knee}}, \\ C, & T_{\text{Knee}} < t \leq T'_{\text{Ground}}. \end{cases} \tag{13}$$

We use the passive swing properties of the leg in the control of the biped robot once again. The knee is allowed to swing freely: when the foot touch sensor detects that the foot departs from the ground, the torque applied at the knee joint is ceased. When the shank comes in line with the thigh, which imply the swing is almost over; a constant torque is applied at the swing knee joint to prepare for the straight leg landing.

To some extent the above controllers can be regarded as reflexes, which are automatic and stereotyped motions programmed in respect to sensory input locally. In addition, these controllers have the same effect as the knee-lock mechanism with locking magnet or latches.[13]

3.3. *Initial conditions leading to a stable limit cycle*

Since the stable biped walking corresponds to a limit cycle in the state space, the biped robot must start from initial conditions within the basin of limit cycle. Considering planar

https://doi.org/10.1017/S0263574709990713 Published online by Cambridge University Press

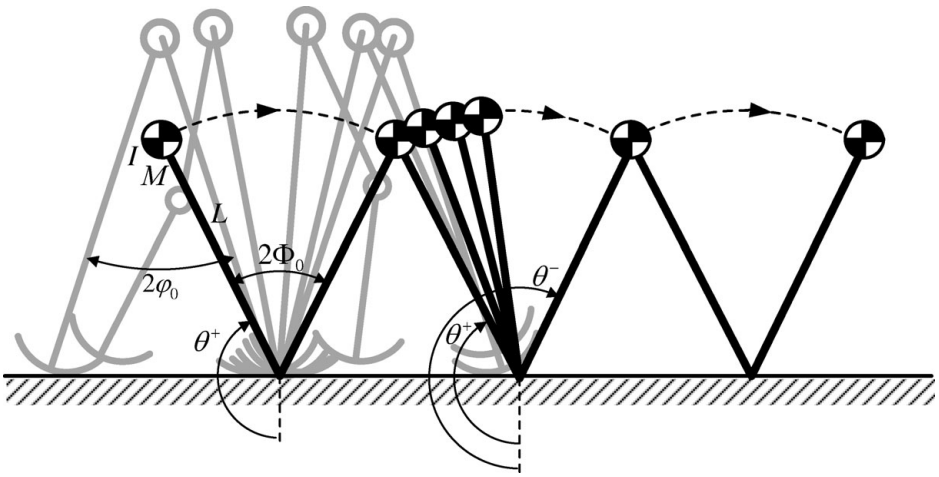


Fig. 6. The simplified model of the task space (an inverted pendulum).

biped walking, the task space is only a single-DOF problem. To obtain the initial conditions that lead to a stable limit cycle, we simplified the task space to be an inverted pendulum, as shown in Fig. 6 Let θ denote the absolute angle of the pendulum, L denote the length from the center of mass (COM) to the pivot point, I denote the inertia about the pivot point, and $M = m_1 + m_2 + m_3$ denote the total mass of the biped robot.

According to the angular momentum balance theorem, the model of the task space has the following special form

$$I\ddot{\theta} = -MgL\sin(\theta). \tag{14}$$

We linearize the Eq. (14) at $\theta = \pi$, and can obtain the analytical solution as

$$\theta = \pi + \frac{\Phi_0}{\sin(\lambda_0 T/2)}\sin(\lambda_0 t), \tag{15}$$

where Φ_0 is the initial pendulum angle as shown in Fig. 6, $\lambda_0 = \sqrt{MgL/I}$, and T is the step period. Therefore, the relationship between the initial angular velocity of the inverted pendulum and the pendulum angle can be written as

$$\frac{\dot{\theta}^+}{\Phi_0} = \frac{\lambda_0}{\tan(\lambda_0 T/2)}. \tag{16}$$

Let $2\varphi_0$ denote the step angle, as shown in Fig. 6. We define initial conditions of the swing leg with $q_1^+ = \pi - \varphi_0$, $q_2^+ = q_3^+ = \varphi_0$ and $\dot{q}_2^+ = \dot{q}_3^+ = 0$ at the beginning of the first phase; therefore, the initial angular velocity of the inverted pendulum can be expressed as

$$\dot{\theta}^+ = \frac{(a_1 + l_1 - 2r)[a_1 - r + (l_1 - r)\tan^2(\varphi_0)]}{2[(a_1 - r)^2 + (l_1 - r)^2\tan^2(\varphi_0)]}\dot{q}_1^+, \tag{17}$$

and the pendulum angle can be written as

$$\Phi_0 = \tan^{-1}\left(\frac{l_1 - r}{a_1 - r}\tan\varphi_0\right). \tag{18}$$

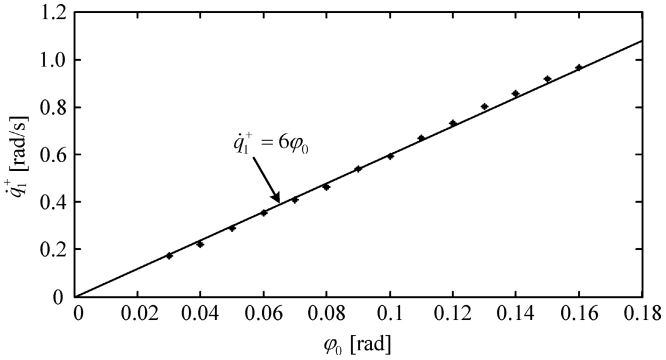


Fig. 7. The relationship between initial angular velocity and the half step angle on the limit cycle.

Taking Eqs. (17) and (18) into Eq. (16), we can obtain the initial angular velocity $\dot{q}_1^+$

$$\dot{q}_1^+ = \frac{\lambda_0}{\tan(\lambda_0 T/2)} \cdot \tan^{-1}\left(\frac{l_1 - r}{a_1 - r}\tan\varphi_0\right) \cdot \frac{2[(a_1 - r)^2 + (l_1 - r)^2\tan^2(\varphi_0)]}{(a_1 + l_1 - 2r)[a_1 - r + (l_1 - r)\tan^2(\varphi_0)]}. \tag{19}$$

Regardless of the swing amplitude, the step period T has a minor change and varies near 0.6 [s]; therefore, we fixed the step period $T = 0.6$ [s] for simplification. From the simulation with link parameters shown in Table I, we found that the stable limit cycle of biped walking can be obtained from any initial value of step length between 0.07 [m] to 0.21 [m]; moreover, we found that the initial angular velocity $\dot{q}_1^+$ is almost linear to the half step angle φ_0 according to Eq. (19), as shown in Fig. 7.

4. Typical Features of Steady Biped Locomotion

We constructed the biped robot model in the simulation environment of Mathworks MATLAB/Simulink R2007b. Figure 8 illustrates the change of angular position and velocity of the support leg in the phase plane with the parameters $A = 0.4$ [Nm], $B = 0.3$ [Nm], $\omega = 2\pi$ and

https://doi.org/10.1017/S0263574709990713 Published online by Cambridge University Press

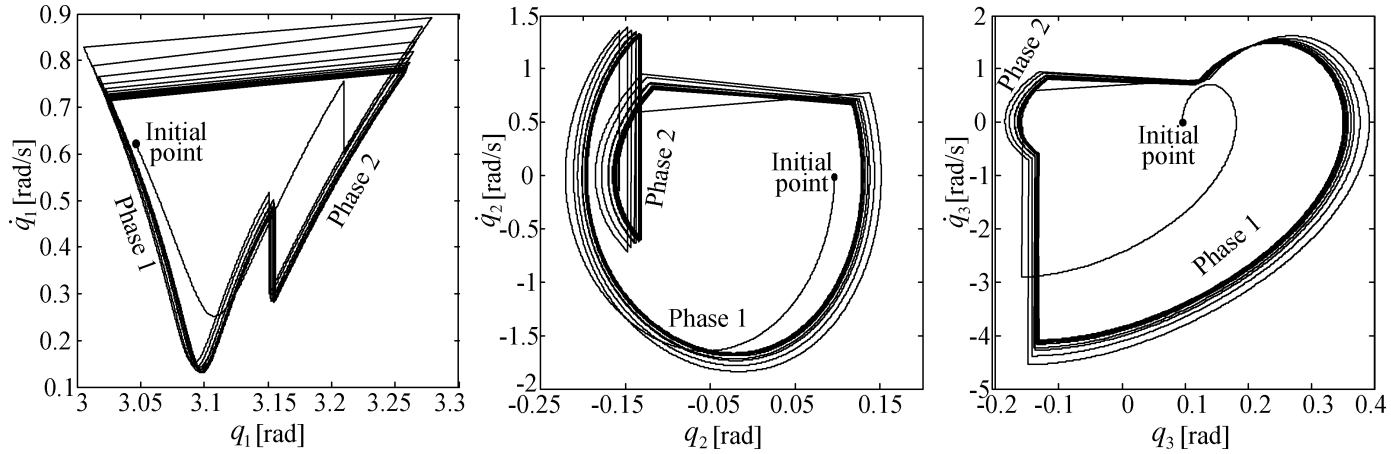


Fig. 8. Phase plane illustration of the support leg with the parameters $A = 0.4$ [Nm], $B = 0.3$ [Nm], $\omega = 2\pi$ and $\varphi_0 = \pi/4$.

$\varphi_0 = \pi/4$. The gaps in the phase plane diagram are due to the collisions at the knee and the ground. We can see from the results that a stable limit cycle is generated by the proposed method. The calculated result is sensitive to the time step in the simulation, because this system contains collision. From the trade-off between calculation accuracy and computing efficiency, the step time of 0.5 [ms] was used in this paper. It also should be noted that, for different initial conditions with same control parameters, the same stable limit cycle is obtained. This indicates that the stable limit cycle is unique for particular control parameters.

Figure 9 portrays the stick figures of the walking behavior with above control parameters. The step period is 0.64 [s], and the postures of the biped is illustrated every 0.07 [s]. We note the shank motion of the swing leg delays from the thigh motion so that the swing foot does not scuff the ground. The velocity of the hip joint is not a constant and decreases to a small value before the support leg passes through the vertical position. This gait pattern is similar to human walking. For the video clip of this simulation, please see Electronic Annex 1 in Appendix C.

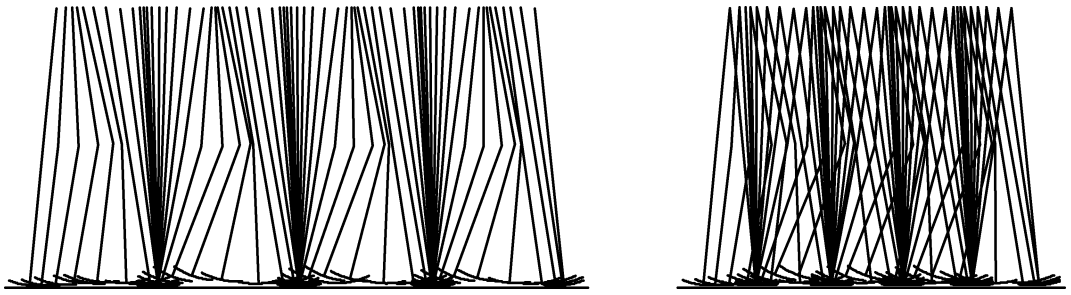
Figure 10(a) and (b) plots the angular displacement of $q_1 - \pi$, q_2, and q_3 and the hip control torque u_h versus the time t respectively. We can see that the hip torque is modulated by touch sensors placed on the foot and the kneecap. It is important to note that the hip control torque shown in Fig. 10 demonstrate that during about one third of step cycle the hip torque is zero, making the biped robot a passive walker during this time. Figure 10(c) demonstrates the input power $P_I(=u_{\{h\}} \cdot (\dot{q}_1 - \dot{q}_2))$ versus time.

To compare efficiency between biped robots of different sizes, it is convenient to use the dimensionless mechanical cost of transport, c_{mt} = (energy used)/(weight × distance traveled).[17,20] Since only the hip control torque performs the mechanical work in our walking strategy, the mechanical cost of transport can be calculated as

$$c_{mt} = \frac{\int_0^{\text{step time}} P_I(t)dt}{(m_1 + m_2 + m_3) \cdot g \cdot \text{step distance}}. \qquad (20)$$

With above control parameters, the mechanical cost of transport c_{mt} is about 0.024. The Cornell biped described by Collins *et al.*[10] walking at $0.4[\text{m} \cdot \text{s}^{-1}]$ has $c_{mt} \approx 0.055$ with 0.8 [m] long legs. The Delft biped walking at $0.4[\text{m} \cdot \text{s}^{-1}]$ achieves a mechanical cost of 0.08 with 0.7 [m] long legs.[10] By measuring oxygen consumption of human beings, biologists estimate that the metabolic cost of transport is about 0.2 at the most economical walking speed. Considering the efficiency of muscles (25%), the corresponding mechanical cost of transport is about 0.05.[20]

The mechanical cost of transport of our walking strategy is even lower than the value actually observed from human beings, and this is partly because that the proposed walking strategy is particularly efficient in the relative low speed. This is different from humans whose most economical walking speed is about $1.3\,[\text{m} \cdot \text{s}^{-1}]$. We conjecture that the reason



(a) (b)

Fig. 9. Stick figures of the walking behavior in simulation. (a) The behavior of one leg during seven steps, and (b) the behavior of two legs during four steps.

https://doi.org/10.1017/S0263574709990713 Published online by Cambridge University Press

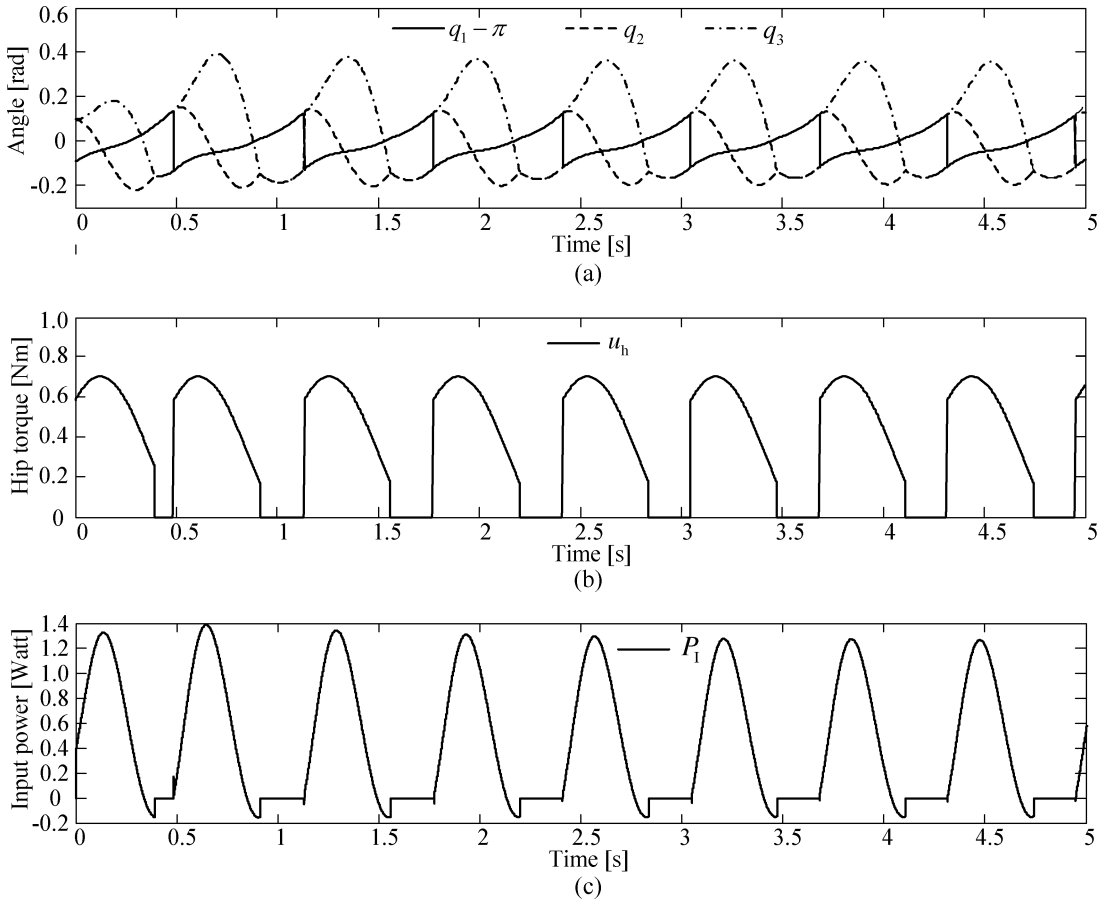


Fig. 10. Angular positions, the hip control torque and input power of the biped robot.

for the above difference is that there is not active actuation in our biped model. In relative high speed (about 0.4 [m · s^{-1}]), the efficiency of the proposed walking strategy is also comparable to the value of humans, and we will give this result in Section 6.3.

It should be noted that, although a mount of electrical energy would be consumed to hold the support knee joint locked in a practical system, we do not take it into account in above calculation because there is no speed in the support knee. This assumption is commonly used to calculate the mechanical cost of this type of robot not only in simulation[13,17] but also in real robots.[10]

In our walking strategy, the support knee joint is controlled by a constant torque to keep the knee straight. To determine the value of the constant torque, the internal constraint torque was inversely calculated using the calculated stable biped locomotion by Newton–Euler Method. As shown in Fig. 11, if the constraint knee torque is negative, the knee can be kept straight by the internal constraint torque without an external torque; however, if the constraint knee torque is positive, the external force is indispensable to keep the knee straight.

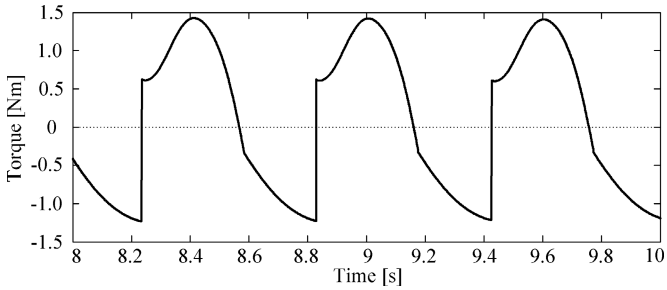


Fig. 11. Internal constraint torque at knee joint of the support leg.

5. Robustness against Oscillator Parameters, Link Parameters, and Environment Variation

5.1. Robustness against oscillator parameters

It is interesting to examine the effect of oscillator parameters and link parameter values on stable walking region. Figure 12 shows the stability region versus oscillator parameters with $\omega = 2\pi$ [rad · s^{-1}]. The shaded areas are the range of oscillator parameters, in which stable gaits appear. We can see from Fig. 12 that a stable walking locomotion can be obtained for a wide range of oscillator parameters, and the stable region is formed between two boundaries. The upper boundary which is plotted in red color can be changed obviously by varying parameter ϕ_0; however, the lower boundary plotted in blue color is indistinctively changed by varying parameter ϕ_0. We note from Fig. 12 that the stable region can be enlarged by increasing parameter ϕ_0.

Walking pattern can be changed on the fly without problems by tuning oscillator parameters as long as they still remain in the stable area shown in Fig. 12. Figure 13 demonstrates angular positions and the hip control input when the oscillator parameter B is changed greatly and

https://doi.org/10.1017/S0263574709990713 Published online by Cambridge University Press

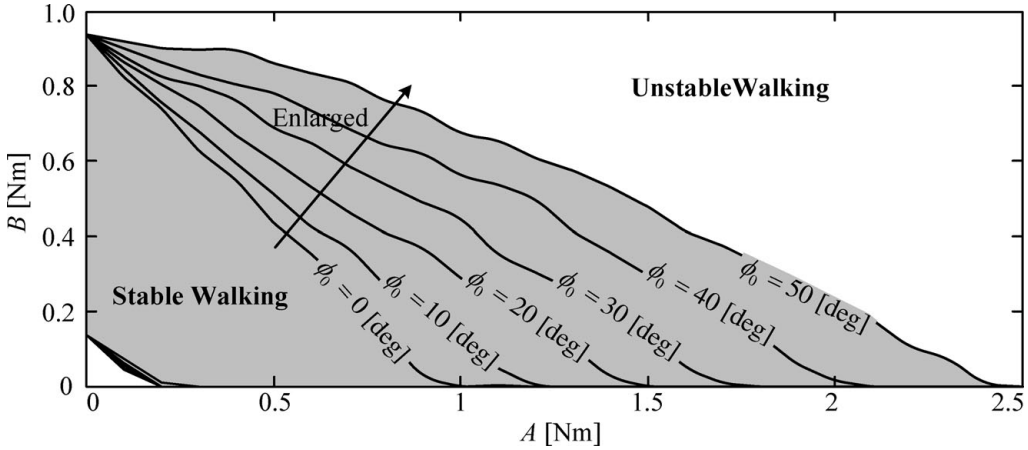


Fig. 12. Transition of stability region of oscillator parameters with $\omega = 2\pi$ [rad · s^{-1}].

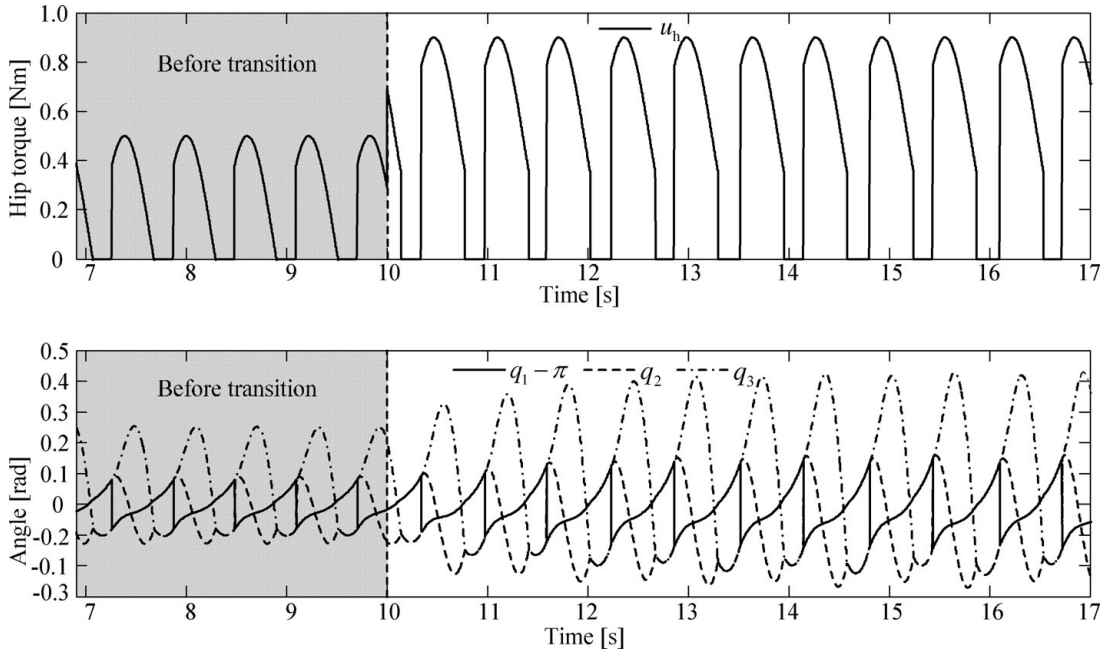


Fig. 13. Angular positions and the hip control input during walking patterns transition when B is changed from 0.1 [Nm] to 0.5 [Nm] at an indicated time instant with a broken line.

abruptly from 0.1 [Nm] to 0.5 [Nm] at a time instant t (indicated with a broken line in Fig. 13). The walking stride is changed from 0.1 [m] to 0.2 [m] within several steps. An interesting thing is that the walking period shows an almost constant value of 0.6 [s] during walking pattern transition. This is because the proposed walking strategy is a natural motion inherent in the biped system. By combining oscillator and passivity of the robot, this simple walking strategy is robust to such drastic parameter variation. Figure 14 plots the corresponding stick figures of walking pattern transition.

For the video clip of this simulation, please see Electronic Annex 2 in Appendix C.

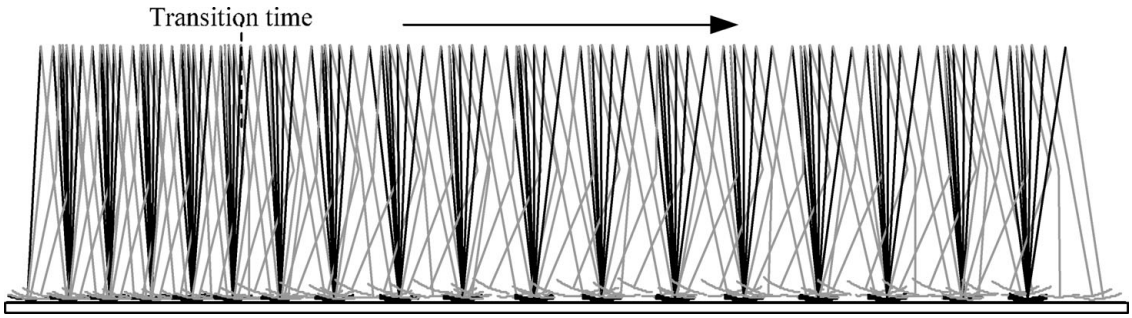


Fig. 14. Stick figures of walking patterns transition (the broken line indicated the transition time).

https://doi.org/10.1017/S0263574709990713 Published online by Cambridge University Press

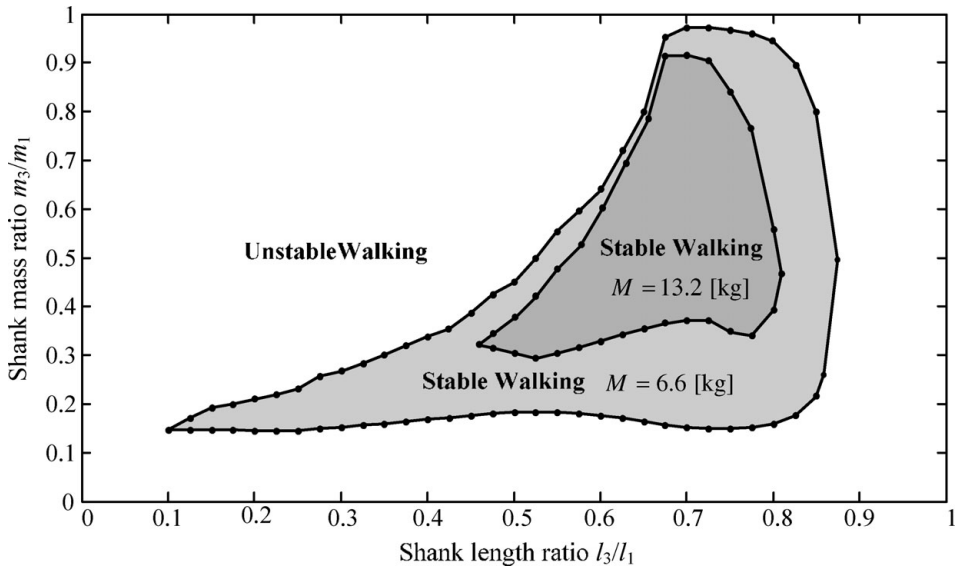


Fig. 15. Stability region of link parameters with oscillator parameters $A = 0.4$ [Nm], $B = 0.3$ [Nm], $\omega = 2\pi$ [rad · s^{-1}] and $\varphi_0 = \pi/4$ [rad].

5.2. Robustness against model inaccuracy

We carried out the link parameter study of the effects of shank length ratio and shank mass ratio on the stability region under the assumption that the total leg length $l_1(= l_2 + l_3)$ is 0.7 [m]. We note from Fig. 15 that the robot can still walk stably when the link parameters vary in a wide range for an invariable oscillator, and this implies that our walking strategy has a good robustness against model inaccuracy. It also should be noted that the stability region shrinks when the total mass increases, as shown in Fig. 15.

5.3. Robustness against environment variation

To evaluate the robustness against environment variation, we change the floor condition, and let the robot walk from a flat ground to a small slope. The robot can walk down a small slope of 2° without adjusting any parameters of the controller. Figure 16 shows the angular displacement, step period and step length while walking down on the slope. After the disturbance, the walking gait soon returns to a new stable orbit. The robot can also walk up a small slope 1° without adjusting any parameters of the controller. Figure 17 shows

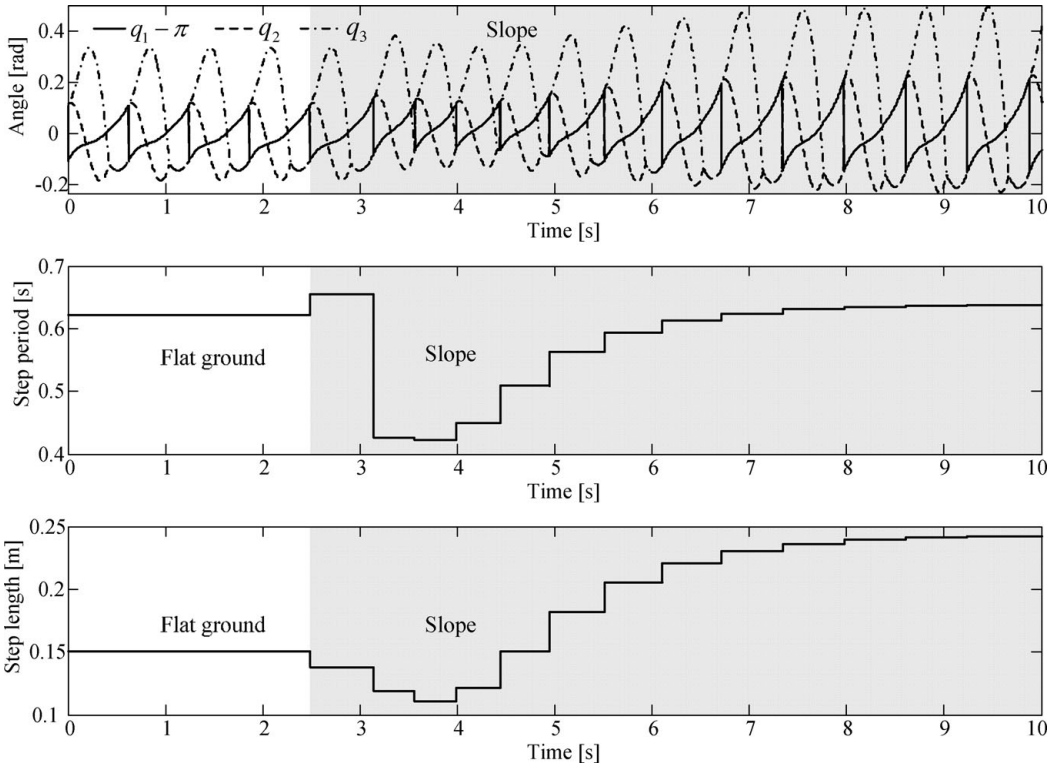


Fig. 16. Walking results of robustness against environment variation (walking down a slope).

https://doi.org/10.1017/S0263574709990713 Published online by Cambridge University Press

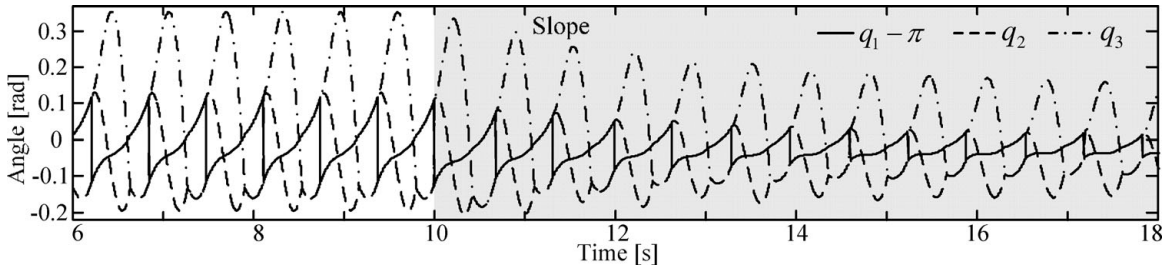


Fig. 17. Walking results of robustness against environment variation (walking up a slope).

the angular displacement while walking up on the slope. This demonstrates that the walking gait is to some degree robust against environment variation with the proposed strategy.

6. Effect of Parameters and Bifurcation Control

In this section, we show the effect of oscillator parameters on four walking indices including step period, walking speed, cost of transport, and foot clearance. We also show the effect of link parameters on the above walking indices, and design a controller to suppress the bifurcation phenomenon.

6.1. Effect of oscillator parameters

We first examine the effect of oscillator parameters on walking indices. Figure 18 shows the step period, walking speed, foot clearance, and cost of transport as functions of oscillator parameters A and B with a fixed $\omega = 2\pi\,[\text{rad} \cdot \text{s}^{-1}]$ and $\varphi_0 = \pi/4[\text{rad}]$. We note from this figure that the larger oscillator bias B is, the larger are the step period, walking speed, foot clearance, and cost of transport. However, bifurcation occurs when B becomes large, and the larger amplitude of oscillator A, is, the smaller is the initial bifurcation point of B. A large value of A has advantages with respect to walking speed and foot clearance; however, a large value of A is bad for energy efficiency. There is a trade-off between speed and efficiency. In addition, whereas the step period shows almost unchanged as A increases.

Figure 19 shows the walking indices as functions of oscillator parameters φ_0 and ω with a fixed $A = 0.3\,[\text{N} \cdot \text{m}]$ and $B = 0.4\,[\text{N} \cdot \text{m}]$. From Fig. 19, we may observe that the smaller initial phase, φ_0, is, the larger are the above four walking indices; however, bifurcation occurs when φ_0 becomes small further. The larger ω is, the smaller is the

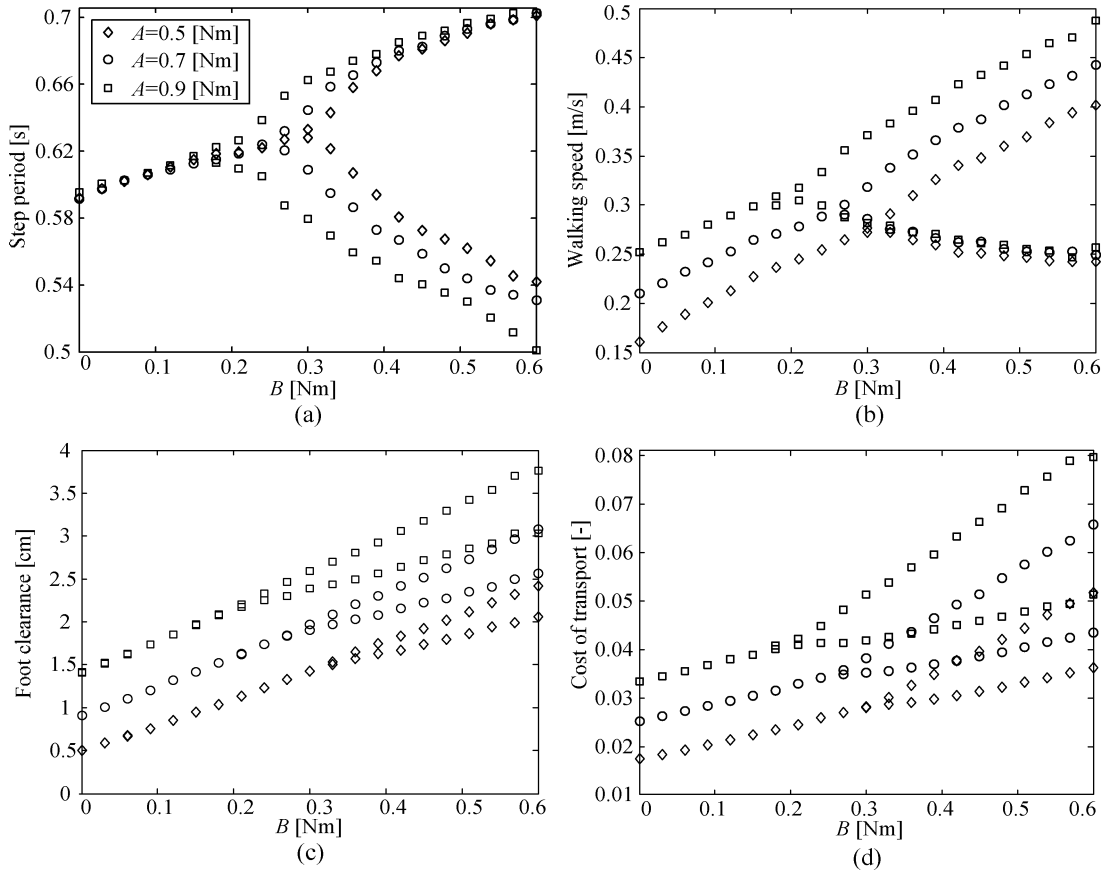


Fig. 18. Effect of the oscillator parameters A and B on walking indices.

https://doi.org/10.1017/S0263574709990713 Published online by Cambridge University Press

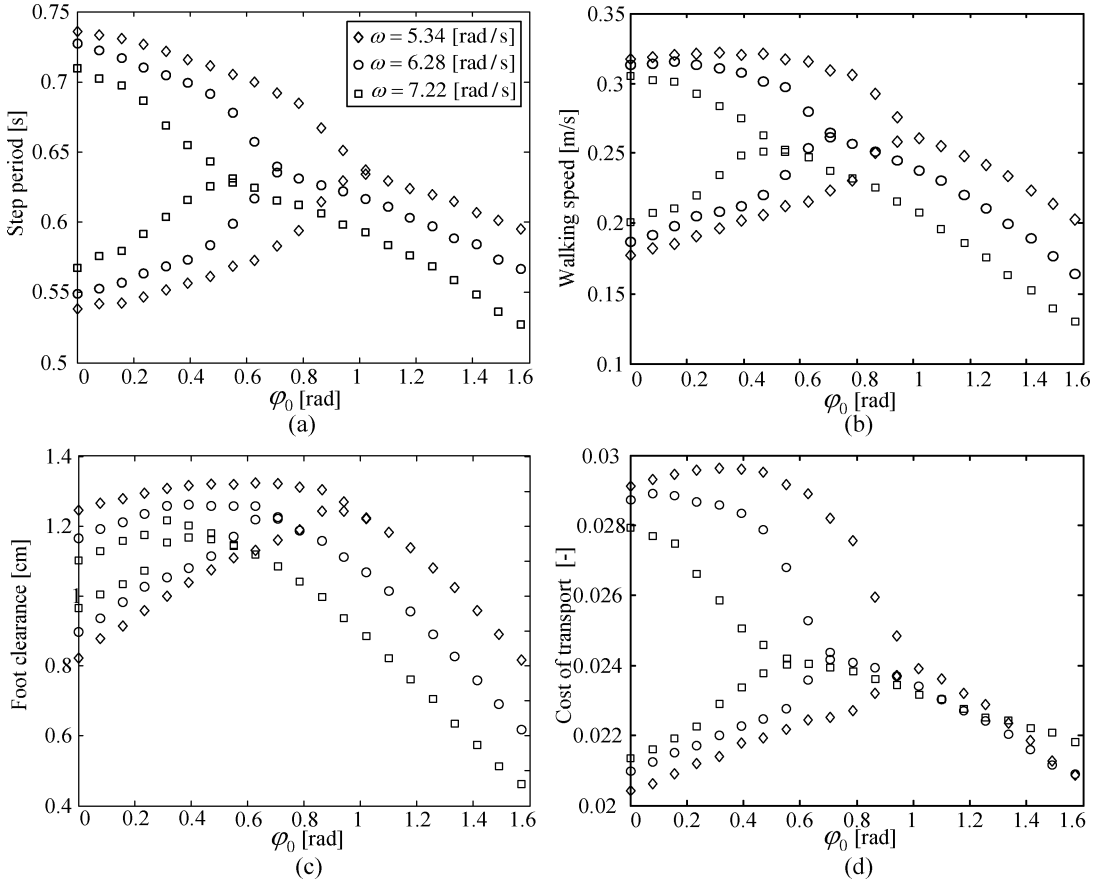


Fig. 19. Effect of the oscillator parameters ω and φ_0 on walking indices.

initial bifurcation point of φ_0. In addition, as ω increases, the values of step period, walking speed, and foot clearance become small.

6.2. *Effect of link parameters*

In this subsection, we analyze the effect of link parameters on the walking indices. To do this, we firstly fixed the shank mass ratio $m_3/m_1 = 0.3333$, and varied the foot radius and the shank length ratio l_3/l_1. Figure 20 shows the simulation results of walking indices with respect to the foot radius and the shank length ratio. From these results, we can see that the large foot radius has advantages of increasing walking speed and decreasing cost of transport; whereas, the large foot radius results in a small foot clearance. There is a trade-off between efficiency and foot clearance when choosing the foot radius.[17] The step period shows almost unchanged as the foot radius increases. In addition, bifurcation occurs when the foot radius increases further, and the larger shank length ratio is, the bigger is the initial bifurcation point of the foot radius. A large shank length ratio has an advantage with respect to walking speed; however, a large shank length ratio is bad for energy efficiency. There is a trade-off between speed and efficiency when choosing the shank length ratio.

Figure 21 shows the simulation results of walking indices with respect to the foot radius and the shank mass ratio with a fixed shank length ratio $l_3/l_1 = 0.5$. We note from this figure that the larger shank mass ratio is, the larger are the step period and energy efficiency. On the other hand, a large shank mass ratio is bad for foot clearance. In addition, the walking speed shows almost unchanged as shank mass ratio increases.

6.3. *Bifurcation control*

From Figs. 18–21, one can see that it is difficult for the biped robot to walk faster than 0.3 $[\mathrm{m}\cdot\mathrm{s}^{-1}]$ with period-one walking mode. As shown in Fig. 18(b), bifurcation occurs when the biped walk faster than 0.3 $[\mathrm{m}\cdot\mathrm{s}^{-1}]$. Based on the error of prior step periods, we design a bifurcation controller to eliminate the bifurcation phenomenon by adjusting the amplitude A and angular frequency ω

$$\begin{cases} A^{i+1} = A^i + K_A \cdot (T^i - T^{i-1}), \\ \omega^{i+1} = \omega^i + K_\omega \cdot (T^i - T^{i-1}), \end{cases} \tag{21}$$

where A^i and ω^i are the amplitude and angular frequency of the oscillator in the ith step, K_A and K_ω are the feedback coefficients, and T^i is step period in the ith step.

To examine the effectiveness of the above bifurcation controller, we choose the oscillator parameters as $A = 0.9$ [Nm], $B = 0.5$ [Nm], $\omega = 2\pi$, and $\varphi_0 = \pi/4$. As shown in Fig. 17(b), the biped walking will lead to a period-two walking mode without bifurcation control. We add the bifurcation controller at 10 [s], and select the feedback coefficient as $K_A = 2.61$ and $K_\omega = 3.09$. Figures 22–24 show the walking results with/without bifurcation control. As shown in Fig. 22, one can see that the bifurcation of step period and step length is almost eliminated within several steps. Figure 23 shows the angular positions and

https://doi.org/10.1017/S0263574709990713 Published online by Cambridge University Press

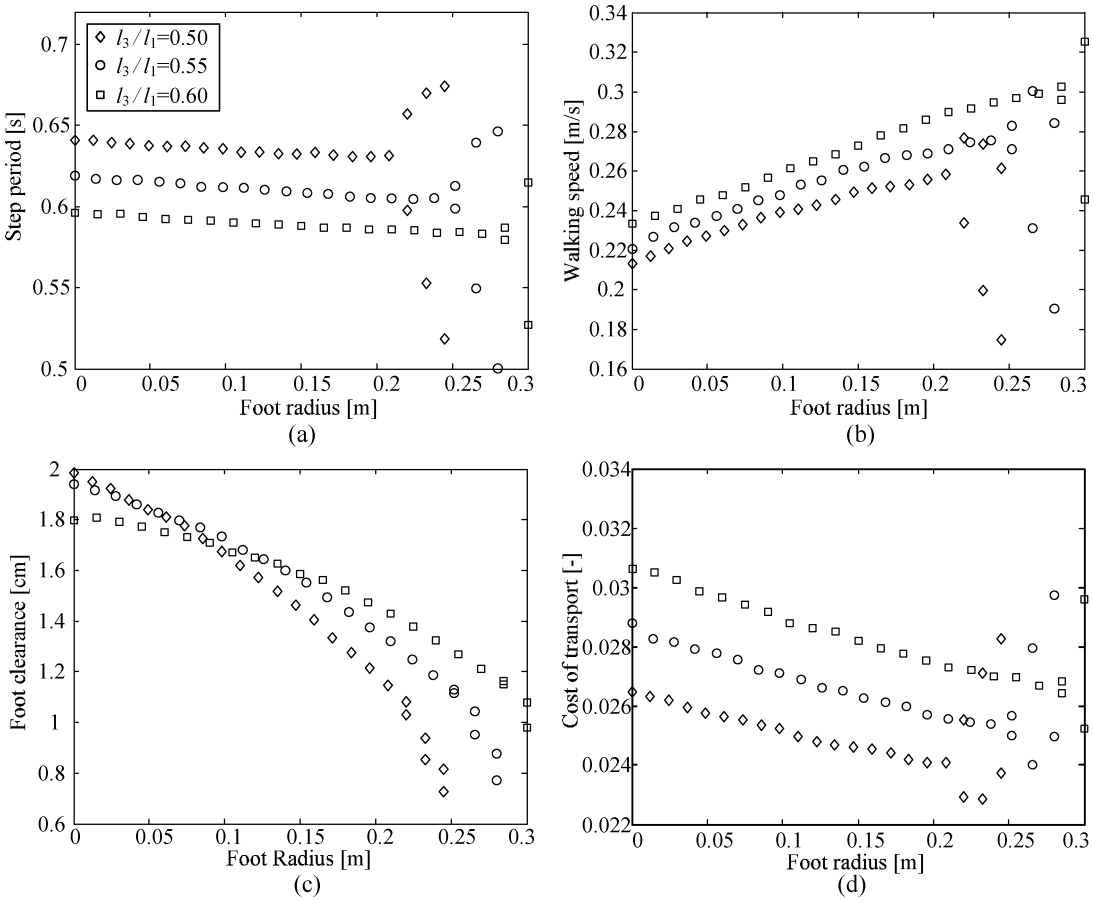


Fig. 20. Effect of the shank length ratio and foot radius on walking indices.

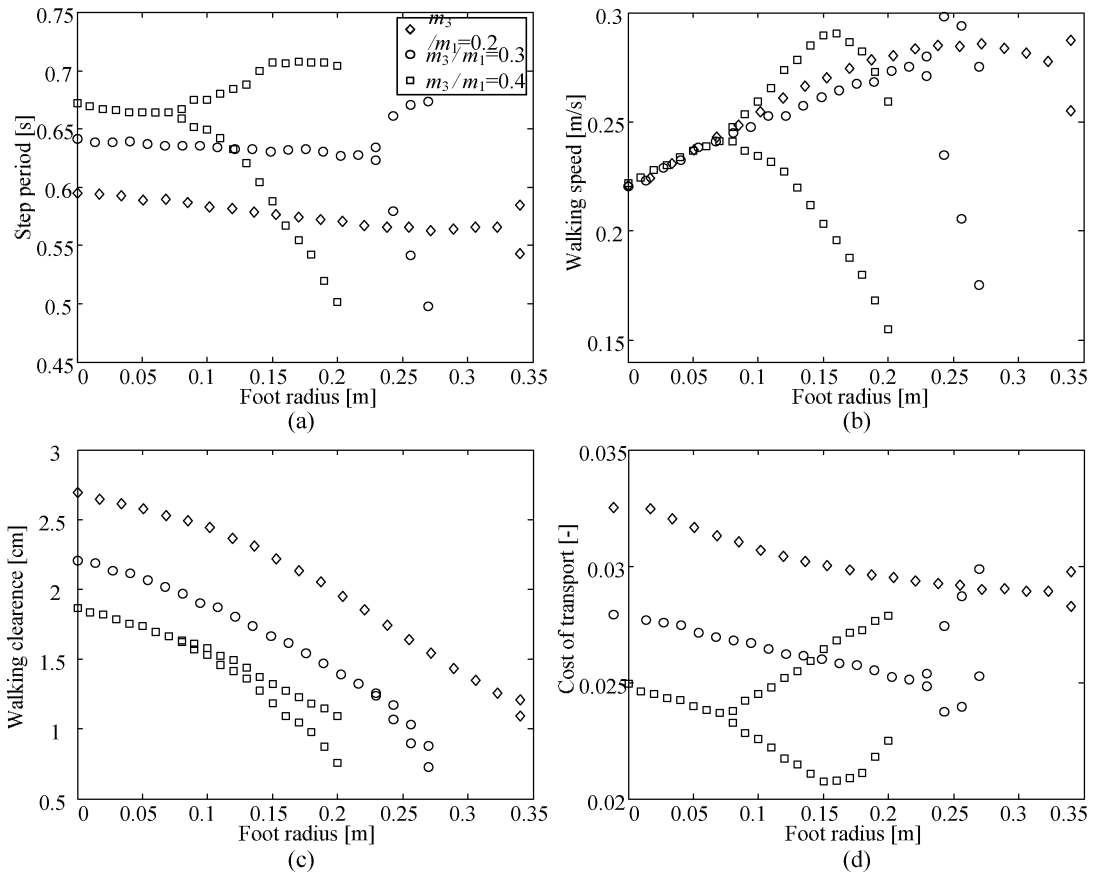


Fig. 21. Effect of the shank mass ratio and foot radius on walking indices.

https://doi.org/10.1017/S0263574709990713 Published online by Cambridge University Press

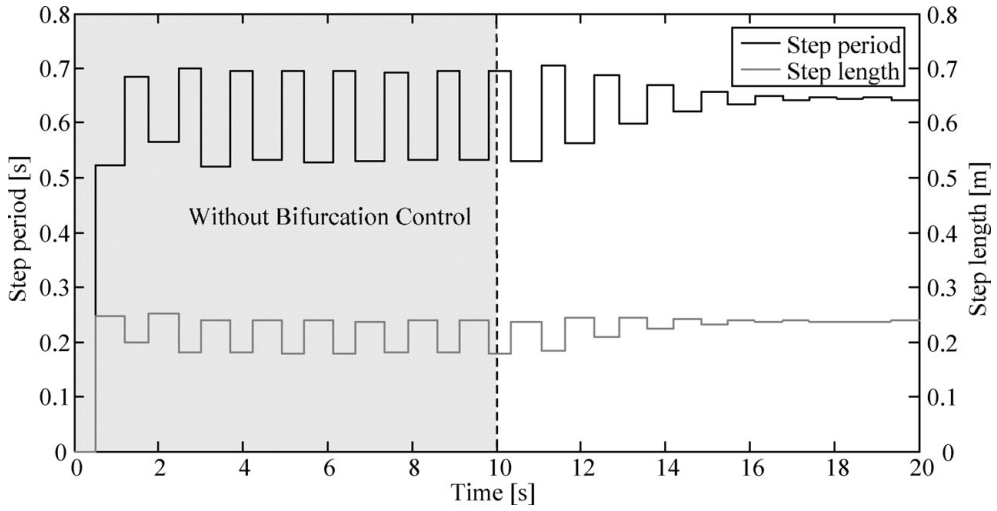


Fig. 22. Step period and step length with/without bifurcation control.

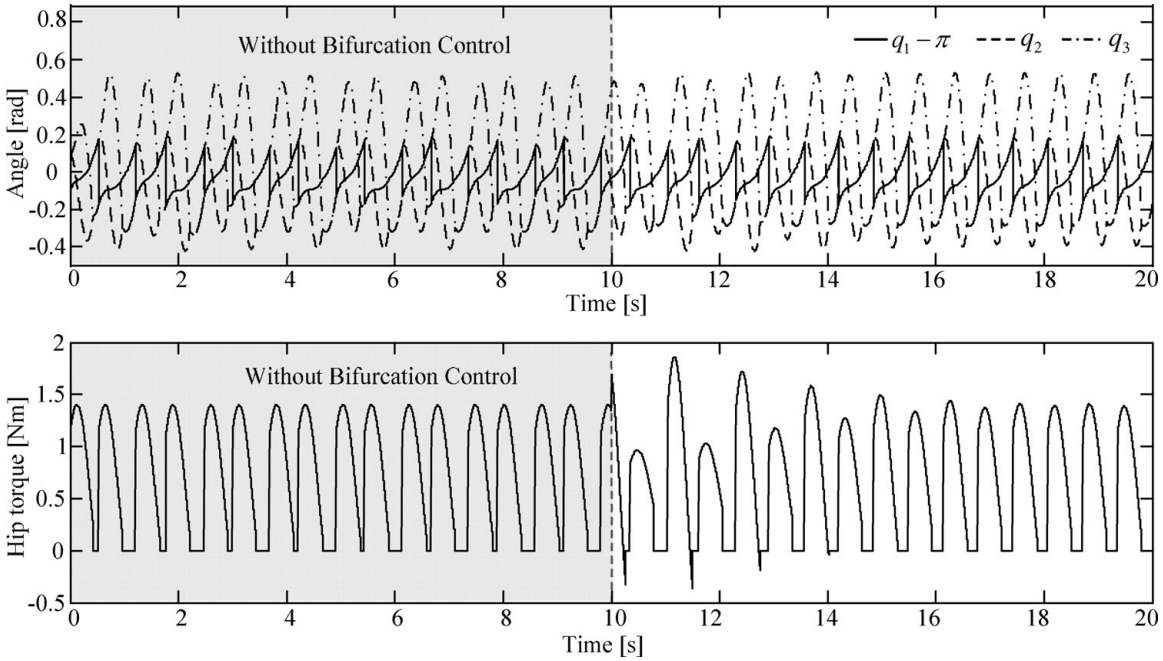


Fig. 23. Angular positions and the hip control torque with/without bifurcation control.

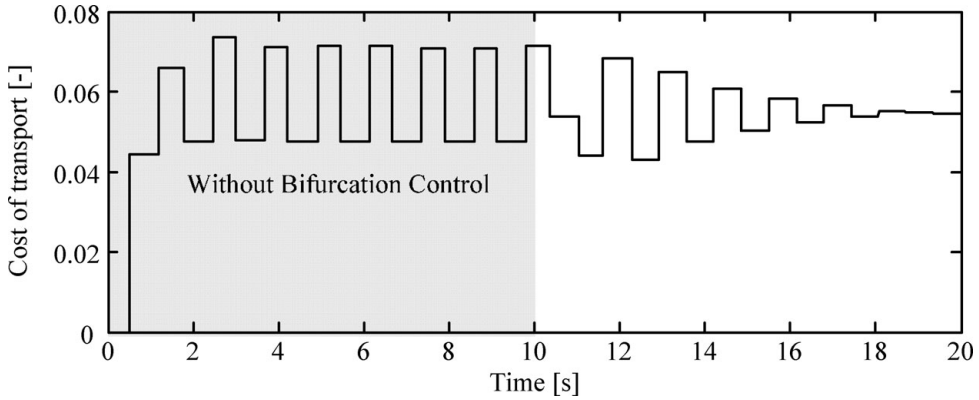


Fig. 24. Angular positions and the hip control torque with/without bifurcation control.

https://doi.org/10.1017/S0263574709990713 Published online by Cambridge University Press

the hip control torque with/without bifurcation control. The walking speed at 20 [s] is more than 0.37 [m · s^{-1}]. Figure 24 shows the corresponding mechanical cost of transport. At the steady walking, the mechanical cost of transport is about 0.054.

For the video clip of this simulation, please see Electronic Annex 3 in Appendix C.

7. Conclusion and Future Work

In this paper, we presented a simple, but efficient and robust walking strategy based on an intermittent sinusoidal oscillator by combination of rhythmic signal and passive dynamic walking. The results of this paper are summarized as follows:

(1) The output of rhythmic signal is simply based on an intermittent sinusoidal oscillator, and few parameters that can be easily tuned. Moreover, stable walking locomotion can be obtained for a wide range of oscillator parameters and link parameters.
(2) We show that the synchronization of biped dynamics can be ensured by triggering/ceasing the rhythmic signal upon the event emitted by two touch sensors placed on the foot and the kneecap respectively, and the passive property of biped walking is utilized by ceasing the rhythmic signal after the swing leg is fully extended.
(3) We demonstrate that the walking strategy is robust against drastic parameter variation and model inaccuracy. We show the basins of attraction for oscillator parameters and link parameters, and we also study the effects of these parameters on various walking indices.
(4) We design a feedback controller to suppress the bifurcation phenomenon occurring at relative high walking speed. We adjust the amplitude and angular frequency of the oscillator based on the error of prior step periods.

We conjecture that the effectiveness of our walking strategy may come from the self-stabilizing properties of biped locomotion. In the future, we will consider combining designated reflexive controllers with our walking strategy in order to increase the walking ability on irregular terrain. In addition, we will conduct experiments with a real biped robot.

Acknowledgment

The first author would like to acknowledge financial support by the National Natural Science Foundation of China under Grant 50805082.

References

1. M. Vukobratovic, B. Borovac, D. Surla and D. Stokich, *Biped Locomotion: Dynamics, Stability, Control and Application* (Springer-Verlag, New York 1990).
2. K. Matsuoka, "Sustained oscillations generated by mutually inhibiting neurons with adaption," *Biol. Cybern.* **52**(6), 367–376 (1985).
3. L. Righetti and A. J. Ijspeert, "Programmable Central Pattern Generators: An Application to Biped Locomotion Control," *IEEE Conference on Robotics Automation*, Orlando, USA (2006) pp. 1585–1590.
4. G. Endo, J. Morimoto, J. Nakanishi and G. Cheng, "An Empirical Exploration of a Neural Oscillator for Biped Locomotion Control," *IEEE Conference on Robotics Automation*, New Orleans, USA (2004) pp. 3036–3042.
5. G. Taga, Y. Yamaguchi and H. Shimizu, "Self-organized control in bipedal locomotion by neural oscillators in unpredictable environment," *Biol. Cybern.* **65**, 147–159 (1991).
6. Y. Fukuoka, T. Mimura, N. Yasuda and H. Kimura, "Integration of Multisensors for Adaptive Walking of a Quadruped Robot," *IEEE Conference on Multisensor Fusion and Integrated Intelligent Systems*, Tokyo, Japan (2003) pp. 21–26.
7. S. Aoi and K. Tsuchiya, "Stability analysis of a simple walking model driven by an oscillator with a phase reset using sensory feedback, " *IEEE Trans. Robot.* **22**(2), 391–397 (2006).
8. J. Morimoto, G. Endo, J. Nakanishi and G. Cheng, "A biologically inspired biped locomotion strategy for humanoid robots: Modulation of sinusoidal patterns by a coupled oscillator model," *IEEE Trans. Robot.* **24**(1), 185–191 (2008).
9. C. Capaday, "The special nature of human walking and its neural control," *Trends Neurosci.* **25**(7), 370–376 (2002).
10. S. H. Collins, A. Ruina, R. L. Tedrake and M. Wisse, "Efficient bipedal robots based on passive-dynamic walkers," *Science* **307**, 1082–1085 (2005).
11. M. Wisse, A. L. Schwab, R. Q. van der Linde and F. C. T. van der Helm, "How to keep from falling forward: Elementary swing leg action for passive dynamic walker," *IEEE Trans. Robot.* **21**(3), 393–401 (2005).
12. S. H. Collins and A. Ruina, "A Biped Walking Robot with Efficient and Human-like Gait," *IEEE Conference on Robotics Automation*, Barcelona, Spain (2005) pp. 1983–1988.
13. K. Ono, T. Furuichi and R. Takahashi, "Self-excited walking of a biped mechanism with feet," *Int. J. Robot. Res.* **23**(1), 55–68 (2004).
14. E. R. Westervelt, J. W. Grizzle and D. E. Koditschek, "Hybrid zero dynamics of planar biped walkers," *IEEE Trans. Autom. Control* **48**(1), 42–56 (2003).
15. T. Geng, B. Porr and F. Worgotter, "Fast biped walking with a sensor-driven neuronal controller and real-time online learning," *Int. J. Robot. Res.* **25**(3), 243–259 (2006).
16. C. Fu and K. Chen, "Gait synthesis and sensory control of stair climbing for a humanoid robot," *IEEE Trans. Ind. Electron.* **55**(5), 2111–2120 (2008).
17. Y. Harata, F. Asano, Z. Luo, K. Taji and Y. Uno, "Biped gait generation based on parametric excitation by knee-joint actuation," *Robotica* **27**(7), 1063–1073 (2009).
18. D. G. E. Hobbelen and M. Wisse, "Swing-leg retraction for limit cycle walkers improves disturbance rejection" *IEEE Trans. Robot.* **24**(2), 377–389 (2008).
19. F. Clarac, D. Cattaert and D. L. Ray, "Central control components of a 'simple' stretch reflex," *Trends Neurosci.* **23**(5), 199–208 (2000).
20. R. M. Alexander, "Walking made simple," *Science* **308**, 58–59 (2005).

Appendix A: Motion Equation for Phase 1

$$D1_{11} = I_1 + m_1 a_1^2 + m_2 l_1^2 + m_3 l_1^2 + 2r(1 + \cos q_1) \times \{r(m_1 + m_2 + m_3) - (m_1 a_1 + m_2 l_1 + m_3 l_1)\}$$

$$D1_{12} = (m_2 a_2 + m_3 l_2)\{(l_1 - r)\cos(q_2 - q_1) - r\cos(q_2)\}$$

$$D1_{13} = m_3 a_3\{(l_1 - r)\cos(q_3 - q_1) - r\cos q_3\}$$

$$D1_{22} = I_2 + m_2 a_2^2 + m_3 l_2^2$$

https://doi.org/10.1017/S0263574709990713 Published online by Cambridge University Press

$$D1_{23} = m_3 a_3 l_2 \cos(q_3 - q_2)$$
$$D1_{33} = I_3 + m_3 a_3^2$$
$$C1_{11} = r \sin q_1 \{(m_1 a_1 + m_2 l_1 + m_3 l_1) - r(m_1 + m_2 + m_3)\}\dot{q}_1$$
$$C1_{12} = -(m_2 a_2 + m_3 l_2)\{(l_1 - r)\sin(q_2 - q_1) - r \sin(q_2)\}\dot{q}_2$$
$$C1_{13} = -m_3 a_3 \{(l_1 - r)\sin(q_3 - q_1) - r \sin q_3\}\dot{q}_3$$
$$C1_{21} = (m_2 a_2 + m_3 l_2)(l_1 - r)\sin(q_2 - q_1)\dot{q}_1$$
$$C1_{23} = -m_3 a_3 l_2 \sin(q_3 - q_2)\dot{q}_3$$
$$C1_{31} = m_3 a_3 (l_1 - r)\sin(q_3 - q_1)\dot{q}_1$$
$$C1_{32} = m_3 a_3 l_2 \sin(q_3 - q_2)\dot{q}_2$$
$$G1_1 = \{(m_1 a_1 + m_2 l_1 + m_3 l_1) - r(m_1 + m_2 + m_3)\} g \sin q_1$$
$$G1_2 = (m_2 a_2 + m_3 l_2) g \sin q_2$$
$$G1_3 = m_3 a_3 g \sin q_3.$$

Appendix B: Motion Equation for Phase 2

$$D2_{11} = I_1 + m_1 a_1^2 + m_1 l_1^2 - 2m_1 r(l_1 + a_1 - 2r) \times (1 + \cos q_1),$$
$$D2_{12} = m_1(l_1 - a_1)\{(l_1 - r)\cos(q_2 - q_1) - r \cos q_2\},$$
$$D2_{22} = I_1 + m_1(l_1 - a_1)^2,$$
$$C2_{11} = m_1 r \sin q_1 (l_1 + a_1 - 2r)\dot{q}_1,$$
$$C2_{12} = -m_1(l_1 - a_1)\{(l_1 - r)\sin(q_2 - q_1) - r \sin q_2\}\dot{q}_2,$$
$$C2_{21} = m_1(l_1 - a_1)(l_1 - r)\sin(q_2 - q_1)\dot{q}_1,$$
$$G2_1 = m_1(a_1 + l_1 - 2r) g \sin(q_1),$$
$$G2_2 = m_1(l_1 - a_1) g \sin(q_2).$$

Appendix C: Electronic Annexes

This paper has supplementary downloadable materials.

Table II. Electronic annexes.

Annexes	Type	Description	
1	Video	Periodic walking animation	http://learn.tsinghua.edu.cn:8080/2007990009/1.avi
2	Video	Walking transition animation	http://learn.tsinghua.edu.cn:8080/2007990009/2.avi
3	Video	Bifurcation control	http://learn.tsinghua.edu.cn:8080/2007990009/3.avi

https://doi.org/10.1017/S0263574709990713 Published online by Cambridge University Press